Available online at www.sciencedirect.com
SCIENCE DIRECT®
Journal of Nuclear Materials 337–339 (2005) 425–430
journal of nuclear materials
www.elsevier.com/locate/jnucmat

Assessment of the poloidal distribution of core plasma fueling and impurity sources in DIII-D

M. Groth [a,*], L.W. Owen [b], G.D. Porter [a], N.H. Brooks [c], M.E. Fenstermacher [a], W.H. Meyer [a], A.W. Leonard [c], T.W. Petrie [c], D.L. Rudakov [d], G. Wang [e], J.G. Watkins [f], N.S. Wolf [a]

[a] *Lawrence Livermore National Laboratory, P.O. Box 808, Livermore, CA 94551, USA*
[b] *Oak Ridge National Laboratory, P.O. Box 2009, Oak Ridge, TN 37831, USA*
[c] *General Atomics, P.O. Box 85608, San Diego, CA 92186, USA*
[d] *University of California, San Diego, 9500 Gilman Drive, La Jolla, CA 92093, USA*
[e] *University of California, Los Angeles, 1040 Veteran Avenue, Los Angeles, CA 90024, USA*
[f] *Sandia National Laboratory, P.O. Box 5800, Albuquerque, NM 87185 USA*

Abstract

Measurements and modeling of the 2D poloidal D_α intensity distribution in DIII-D low density L-mode and medium density ELMy H-mode plasmas indicate that the core plasma is predominately fueled near the divertor X-point region. The neutral deuterium and ion carbon emission were measured in the divertor and inner main chamber scrape-off layer (SOL) using a plasma imaging technique, covering 85% of the poloidal cross-section. Typically, the peak emission in the inner main SOL at the tokamak midplane was three orders of magnitude lower than in the divertor. For discharges with the ion $\boldsymbol{B}\times\nabla B$ drift direction toward the lower divertor the UEDGE/DEGAS codes predict strong core plasma fueling from the significantly higher density and lower temperature plasma calculated in the inner divertor leg. The concomitant carbon ion flow reversal in the inner divertor leg enhances the leakage of carbon from the divertor into the main SOL, and hence into the core.

PACS: 52.40.Hf; 52.65.y; 52.70.m
Keywords: Fueling; Carbon transport; Poloidal drifts; Plasma imaging; DIII-D

1. Introduction

The poloidal divertor configuration in toroidal magnetic fusion devices was designed to maximize plasma-wall contact with the plasma facing components (PFCs) at the divertor target plates, and to inhibit impurities produced at the divertor target from reaching the main plasma. Understanding and controlling the recycling processes at the plasma surrounding walls is important for future devices to achieve the desired performance and plasma purity. The poloidal distribution of the core fueling source is considered to be a crucial factor in the formation of the H-mode pedestal [1]. The divertor region, i.e. the region downstream from the X-point, as

* Corresponding author. Address: General Atomics, P.O. Box 85608, San Diego, CA 92186, USA. Tel.: +1 858 455 4183; fax: +1 858 455 4156.
E-mail address: groth@fusion.gat.com (M. Groth).

0022-3115/$ - see front matter © 2004 Elsevier B.V. All rights reserved.
doi:10.1016/j.jnucmat.2004.09.068

well as the vicinity of the X-point, was conceived as the dominant particle source fueling the core plasma. While this description was shown to hold in tokamak experiments [2], and is also confirmed in this paper, recent results, in particular from the Alcator C-Mod tokamak [3], indicate that a significant ion flux in the scrape-off layer (SOL) may reach the main chamber wall.

This paper assesses particle recycling in the DIII-D tokamak by relating experimental measurements and 2D computational modeling to particle transport in the divertor and main SOL region. Multiple edge diagnostics were used to measure the 2D neutral particle (D_α) and carbon ion (CII/CIII) emission distribution in both the divertor and main diagnostic chamber region. The main tool of this paper is tangentially viewing charge injection device (CID) cameras [4,5], from which time-averaged 2D poloidal D_α, CII (514 nm), and CIII (465 nm) distribution profiles were inferred, covering approximately 85% of the DIII-D poloidal cross-section (Fig. 1). Other diagnostics include vertically and tangentially viewing photomultiplier (PMT) systems [6], Langmuir probes embedded in the lower divertor target plates [7], and two Thomson scattering systems in the core, main SOL, and divertor region [8,9]. The intensity distributions of the D_α, CII, and CIII emission were simulated using the edge fluid code UEDGE [10] and neutral transport code DEGAS [11]. Core plasma fueling, core impurity sources, and impurity transport were extracted from the code solutions. Detailed comparison of the experimental results with the transport models are presented for two operating regimes: (i) low-density L-mode discharges, discussed in Section 2, and (ii) medium-density ELMyH-mode discharges addressed in Section 3. These results are summarized and further discussed in Section 4.

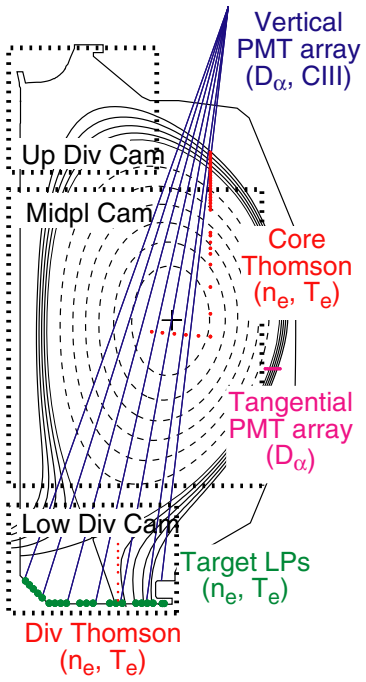

Fig. 1. Subset of the DIII-D edge diagnostic system referred to in this paper. The magnetic configuration of the low density L-mode discharge (shot 110465 at 3500 ms) is also shown. Other discharge parameter include total heating power, P_{tot} = 0.9 MW, toroidal field, B_T = 2.0 T, and plasma current, I_p = 1.1 MA.

2. Measurement and modeling of low-density L-mode plasmas

2.1. Methodology and experimental results

Analysis of DIII-D plasmas with the full set of tangential cameras was performed in low-density ($\bar{n}_e = 2.1 \times 10^{19}$ m^{-3}, $n/n_{GW} = 0.2$), low-confinement (L-mode) discharges [12]. The plasma configuration is shown in Fig. 1, i.e., a lower single-null (LSN) with the ion $\boldsymbol{B} \times \nabla B$ drift direction toward the lower divertor. Particle control was provided by initial gas puffing and wall pumping. To optimize diagnostic spatial resolution of the outer divertor plasma, the outer strike point (OSP) was swept across the Langmuir probes (LPs), and the view chords of the lower PMT arrays and divertor Thomson scattering (DTS). The inner strike point was held on the DIII-D center post. The separatrix-to-wall gaps at the inner and outer tokamak midplane were also held constant at 13 cm and 8 cm, respectively, during the OSP sweep.

The temperature measured by Langmuir probes and divertor Thomson scattering, $T_{e,LP-OSP} \sim 35$ eV, resp. $T_{e,DTS-OSP} \sim 20$ eV, indicates that the outer divertor plasma was well-attached to the target plates. Consistently, the intensity distribution of CII and CIII light strongly peaks at the OSP at the target plate. In contrast, the CIII emission from the inner divertor leg was measured well off the center post, indicating that the plasma temperature in the inner divertor leg is below 5 eV (Inner divertor LP or DTS measurements were not available for this configuration.). The D_α emission extends poloidally about 20 cm into the inner divertor plasma Fig. 2(b)]. Using the 2D distribution profile from the camera data, obtained by tomographic reconstruction, the calculated line-integrated signals along the view chords of the vertical PMT were consistent in spatial distribution as well as in absolute magnitude with the measured values.

The D_α CII, and CIII intensity distribution measured in the high-field side SOL around the device midplane ($0.7\text{ m} < Z < 0.7$ m), herein called the inner main SOL, is strongly peaked towards the lower divertor X-point

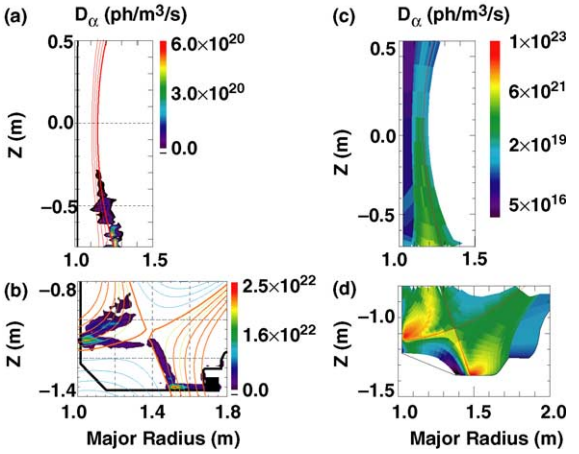

Fig. 2. Experimental (a and b) and UEDGE/DEGAS simulated (c and d) D_α emission distribution in the high-field main SOL (a and c) and lower divertor (b and d) for reference L-mode discharge 110465.

[D_α Fig. 2(a)], suggesting that the particle source is in the inner divertor region. The measurements show that the D_α emission is close to or at the separatrix, while CII and CIII emission are only observed in the SOL. Typically, the emissivity decreased over a poloidal scale length of 0.1 m (D_α), 0.2 m (CII), and 0.3 m (CIII). This poloidal scale length was calculated by taking the peak emissivity in the inner main SOL as a function of vertical distance along the center post. This method is approximate since the field lines are nearly parallel to the centerpost in this region of the plasma. The peak emissivity in the SOL above the X-point was approximately two orders of magnitude lower than at the inner strike point. If the inner main wall is a dominant particle source, then one should expect a much more uniform or poloidally symmetric intensity distribution.

2.2. Core fueling poloidal profile and carbon transport using UEDGE/DEGAS

The above measurements were well reproduced using the UEDGE and DEGAS codes, which calculate that fueling through the divertor X-point region is the dominant core plasma fueling mechanism. The edge fluid code UEDGE was executed using a classical transport description with $\boldsymbol{B}\times\nabla B$ and $\boldsymbol{E}\times\boldsymbol{B}$ drifts [13], and a purely diffusive radial transport model with spatially constant diffusivities. The anomalous diffusivities were obtained by matching the experimental core and main SOL electron temperature and density measured by the core Thomson system: $D_\perp = 0.2$ m^2/s, $\chi_e/\chi_i = 0.8$ m^2/s. In UEDGE, a unity recycling coefficient was used for the hydrogen ions and neutrals at the divertor target. A neutral albedo of 0.95 was applied along the outer UEDGE boundary to allow finite wall pumping. Carbon neutrals were produced by physical and chemical sputtering at the target plates, and by chemical sputtering only at the outer grid boundary, using sputtering yields obtained from the Toronto database [14]. The ion transport of each charge state was modeled using a force balance equation [15].

Based on the UEDGE plasma solution, the D_α emission calculated by DEGAS peaks at the ISP, and is approximately three orders of magnitude lower in the high-field SOL at tokamak midplane ($Z = 0$). The neutral Monte-Carlo code DEGAS was used to model the neutral hydrogen particle transport, due to wall reflection and charge exchange, from the divertor to the main chamber in realistic DIII-D geometry [16,17]. In these simulations particles were launched only from the divertor targets, since the radial ion fluxes across the radially outermost grid boundary as calculated by UEDGE are 2–3 orders of magnitude lower than those to the divertor target plates. For the region between the outer UEDGE domain boundary and the DIII-D wall, a constant electron density and temperature equal to one half of the UEDGE solution at $\psi = 1.1$ was assumed. The calculated D_α emission peaks at the ISP, but extends far into the inner divertor leg Fig. 2(d)]. In the main chamber Fig. 2(c)], the peak emissivity at $Z = 0.7$ m is approximately one hundredth of peak emissivity at the ISP. The calculated characteristic poloidal decay length of D_α is 0.15 m, consistent with the measurements. Similar to [17], the measured D_α emission in the outer main SOL is well reproduced using a wall pumping coefficient of 0.36 in DEGAS. With zero wall pumping, DEGAS overestimates the D_α emission by a factor 2–5, indicating that additional recycling of ions at the main chamber wall would be an excessive source.

The DEGAS poloidal distribution of the neutral flux into the core plasma, shown in Fig. 3, reveals that approximately 70% of the core fueling comes from neutrals born in the divertor region. Here, we define a divertor region that extends two charge-exchange mean free paths (~20 cm) above the divertor X-point, since neutrals that penetrate into the core from the main SOL in this region previously originated in the divertor. The remaining 30% of the core fueling arises from neutral leakage out of the divertor. Two key effects arise from the significantly colder plasma in the inner divertor leg, namely, the flow reversal away from the divertor plates, and the reduced ionization of divertor produced neutrals. The result of these effects accounts for inner leg fueling twice that of the outer divertor leg.

The UEDGE simulations reproduced the poloidally non-uniform CII and CIII midplane distribution, and indicated that the divertor walls are the carbon sources that set the upstream carbon density. Here, the divertor walls are defined as the outermost UEDGE boundary in the SOL, extending from the target plates to about

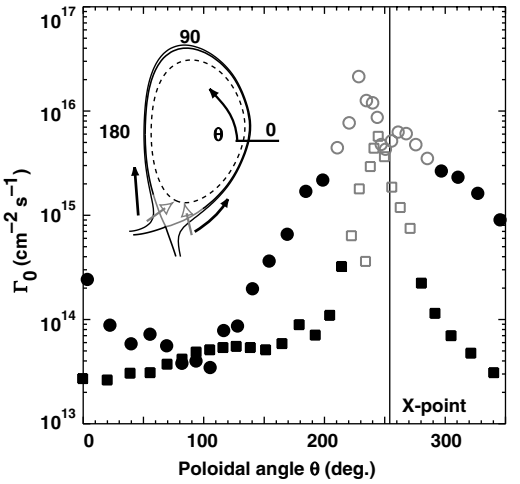

Fig. 3. Calculated DEGAS neutral flux into the core as a function of poloidal angle for L-mode (○) and ELMy H-mode plasmas (□). The open (grey) symbols indicate X-point fueling, the closed symbols fueling due to divertor neutral leakage. The poloidal angle is measured counter clockwise from the outer midplane (see insert).

20 cm above X-point. The UEDGE code predicts increased chemical sputtering of carbon, since the neutral density in the region upstream of the strike points is high. Chemical sputtering of carbon is also enhanced at the UEDGE boundary to the private flux region. Sputtered carbon material from the target plates is mostly redeposited onto the plates. The dynamics of carbon transport in the lower divertor is complex (Fig. 4), and can be described by the following processes. Carbon

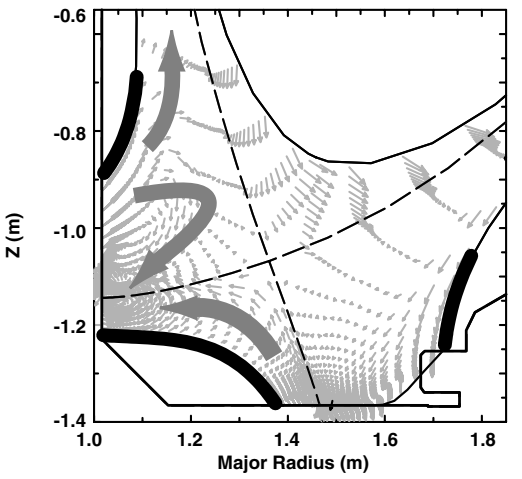

Fig. 4. Flux of carbon in the divertor summed over all ionization stages as calculated by UEDGE. The arrows illustrate the main flow direction in the lower divertor. The divertor walls are highlighted by the thick black lines.

is swept from the private flux region to the inner divertor leg due to $\boldsymbol{E}\times\boldsymbol{B}$ associated drifts from the large radial electric field near the separatrix. The inner divertor leg is a region of strong reversed flow: in the far-SOL region carbon flows upstream, while in the region near to the separatrix carbon is swept towards the target plates by the background plasma flow. Above $Z = 0.8$ m, the ion temperature gradient force exceeds the frictional drag of the background plasma, and carbon ions get transported into the main SOL.

3. Measurement and modeling of ELMy H-mode plasmas

3.1. Comparison of experimental intensity distribution in LSN, USN, and DN plasmas

Poloidally non-uniform D_α CII, and CIII intensity profiles, with the maximum emission near the divertor X-point region were also observed with the midplane tangential camera in ELMy H-mode plasmas with varying magnetic configuration and ion $\boldsymbol{B}\times\nabla B$ drift. For similar pedestal parameters ($n_{e,ped} = 4.5\times10^{19}$ m^{-3}, $T_{e,ped} = 450$–900 eV) three different plasma configurations with the ion $\boldsymbol{B}\times\nabla B$ drift into the upper divertor were executed [Fig. 5 (insert)]: an upper single-null (USN), double-null (DN), and lower single-null (LSN)

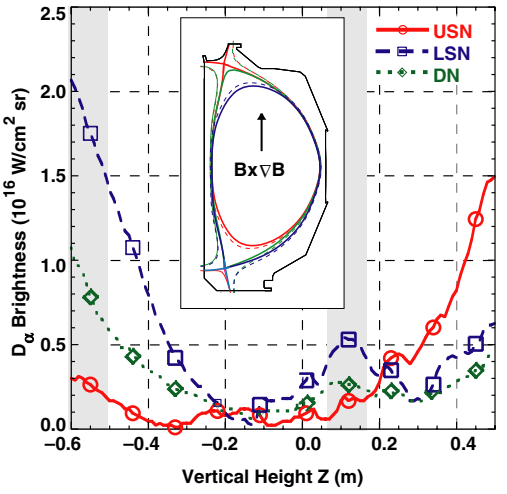

Fig. 5. Comparison of the peak D_α emission in the inner main SOL as a function of vertical height around the midplane, $Z = 0$, for USN, DN, and LSN discharges with the ion $\boldsymbol{B}\times\nabla B$ drift into the upper divertor. Typical plasma parameters include $P_{NBI} = 5.5$ MW, $H_{89} \sim 2$, $B_T = 2.0$ T, $I_p = 1.3$ MA, and $\bar{n}_e = 5.2\times10^{19}$ m^{-3} ($n/n_{GW} = 0.4$). The region of interest includes the in the inner main SOL as measured by the midplane camera system (Fig. 1). The shaded areas indicate regions that were possibly affected by reflections of light from the lower divertor. Insert: USN, DN, and LSN equilibria used for studies of ELMy H-mode plasmas.

configuration of magnetic balance 4 cm, 0, 4 cm, respectively. The same three magnetic configurations were repeated with the reversed toroidal field direction changed so that the ion $\boldsymbol{B}\times\nabla B$ drift direction was toward the lower divertor. DIII-D is a two-divertor tokamak, with a relatively open divertor structure in the lower vessel region, and a more closed upper divertor structure. In the context of this paper, we define the active divertor as the one closest to the magnetic X-point. For the $\boldsymbol{B}\times\nabla B$ drift into the upper divertor, the peak D_α emission in the inner main SOL was measured in the region closest to the active divertor X-point for SN cases, and close to both X-point regions in the DN case (Fig. 5). Using the midplane camera data alone, the emission decreased by an order of magnitude from the divertor X-point region ($Z = -0.6$ m) to the midplane ($Z = 0$). The data from the divertor and midplane cameras show the peak emissivity in the active divertor is approximately two to three orders of magnitude higher than in the inner main SOL, and about one to two orders of magnitude higher than in the passive divertor. In comparison, the peak CII emission in the active divertors was approximately two orders of magnitude higher than in the passive divertors and in the inner main SOL. Because these SN configurations had a passive X-point within the vacuum vessel, there is still significant plasma wall interaction in the passive divertor, observed predominately in the outer divertor leg. These observations were independent of the magnetic configuration and ion $\boldsymbol{B}\times\nabla B$ drift direction. In those configurations with the ion $\boldsymbol{B}\times\nabla B$ drift direction pointing into the active divertor, the D_α emission peaked in the higher density, lower temperature inner divertor leg, produced by the $\boldsymbol{E}\times\boldsymbol{B}$ particle drift in the private flux region. Consistently, the measured CIII emission, elongated along the inner divertor leg, but peaked at the OSP in the outer leg, indicated a lower plasma temperature in the inner leg than in the outer leg. In those configurations with the ion $\boldsymbol{B}\times\nabla B$ drift pointing out the active divertor, D_α CII, and CIII emission in the active divertor was similar in the inner and outer divertor leg.

3.2. Comparison of measurement and UEDGE/DEGAS modeling in LSN ELMy H-mode plasmas

The distinctively different D_α intensity distributions measured in the lower divertor for the two $\boldsymbol{B}\times\nabla B$ drift directions was consistently reproduced in UEDGE with the $\boldsymbol{B}\times\nabla B$ and $\boldsymbol{E}\times\boldsymbol{B}$ terms included in the calculations, and not reproduced in simulations without the drifts. This emphasizes the importance of incorporating these processes in the modeling. The spatially constant diffusivities used for the radial transport in the H-mode cases were lower than for the L-mode case, i.e., $D_\perp = 0.0875\ \mathrm{m^2/s}$, $\chi_e = \chi_i = 0.35\ \mathrm{m^2/s}$. Unity recycling was assumed for ions striking the divertor plate or radially outermost computational boundary cells. To allow finite wall pumping, a neutral albedo of 0.98 was applied along the outer UEDGE boundary up to 10 cm above the divertor plates, and 0.95 elsewhere. Carbon was introduced by physical and chemical sputtering at the target, and chemical sputtering at the radial outermost UEDGE boundary.

In LSN discharges with the ion $\boldsymbol{B}\times\nabla B$ drift into the lower divertor (Case A), the $\boldsymbol{E}\times\boldsymbol{B}$ induced particle flow in the private flux region causes significant asymmetry in the electron and ion density and temperature profile in the inner and outer divertor leg, resulting in higher D_α emission in the inner divertor leg. The UEDGE code predicts a region of flow reversal, i.e. flow of carbon ions away from the target plates, in the inner divertor leg, enhancing the leakage of carbon ions from this region into the main SOL. In LSN discharges with the ion $\boldsymbol{B}\times\nabla B$ drift out of the lower divertor (Case B), a region of strong flow reversal is calculated by the code in the outer divertor leg. However, a much more symmetric density and temperature profile is calculated for the inner and outer divertor leg, consistent with the D_α and CII measurements. Away from the divertor UEDGE predicts a significantly stronger CII emission in the inner main SOL for Case A, which was not conclusively measured by the midplane camera. For both cases, CII emission decreases poloidally toward the midplane, in agreement with the experiment.

The spatial distribution of the D_α emission calculated by DEGAS using the UEDGE background plasma of Case B is consistent with the measured emission in the lower divertor, the inner main SOL, and the outer midplane SOL. The peak D_α emissivity at the ISP is approximately three orders of magnitude higher than at the midplane. In the outer midplane SOL, the tangential PMT array measuring D_α is reproduced by DEGAS within a factor of 2 in the SOL using the following parameters for the region outside the UEDGE domain: $n_{e,halo} = 0.5\, n_{e,UEDGE,\psi=1.1}$, $T_{e,halo} = T_{i,halo} = T_{e,UEDGE,\psi=1.1}$. ($\psi = 1.1$ is the normalized flux at the radially outermost UEDGE grid cells.) Radially inboard from the separatrix the measured D_α emission is a factor of 5–8 lower than that calculated by DEGAS. The poloidal distribution of the neutral flux into the core calculated by DEGAS is strongly peaked around the divertor X-point (Fig. 3). Based on this distribution, the core fueling across the X-point region is approximately 10 times larger than through leakage of neutrals into the main chamber, consistent with UEDGE modeling results shown previously [18,19].

4. Summary and discussion

Two-dimensional poloidal emission distributions from tangentially viewing camera measurements,

combined with UEDGE/DEGAS simulations, that also reproduce measurements from multiple diagnostics, indicate that divertor recycling is the dominant particle source for the core in DIII-D low density L-mode and ELMy H-mode plasmas. The computational simulations matched a large set of experimental data by application of a purely diffusive radial transport model in UEDGE, and use of this solution as input for DEGAS to calculate particle fueling and neutral leakage. In these simulations the D_α intensity distribution in the divertor as well as in the inner main and outer midplane SOL were reproduced with recycling imposed only at the divertor target plates. The measured D_α CII, and CIII distribution in the divertor were consistently reproduced, only when the effects of $\boldsymbol{B}\times\nabla B$ and $\boldsymbol{E}\times\boldsymbol{B}$ drifts were included in UEDGE. In plasmas with the ion $\boldsymbol{B}\times\nabla B$ drift into the divertor, the significantly higher density and lower temperature in the inner divertor leg provides a strong fueling source to the main plasma. Since core plasma performance is determined by the pedestal temperature, and the pedestal pressure is set by ELM stability, more effective control of the pedestal density may be provided through divertor pumping in this fueling regime, than in the case of main chamber recycling.

The poloidal distribution of sputtered carbon along the separatrix shows peaking towards the divertor X-point, which may allow enhanced impurity screening in future devices. Flow reversal in the inner divertor leg away from the target enhances the leakage of carbon ions out of the divertor into the main SOL.

While these results are encouraging, because they suggest that the dominant impurity source is the divertor region and not the main walls, the same set of experimental data needs to be confronted with models that invoke main chamber recycling [20,21]. Those models are motivated by the measurement, in some discharges, of significantly higher plasma densities and temperatures at a single poloidal location in the far SOL than predicted by simple diffusive models. Increased main chamber interaction is predominately observed in high-density ($n/n_{GW} \rightarrow 1$) L-mode operation, while this paper addresses low to medium density regimes. Clearly, better poloidally (and toroidally) distributed measurements of n_e and T_e in the main SOL are needed to identify the differences in the SOL plasma conditions that produce both of these observations.

Acknowledgment

This work was performed under the auspices of the US Department of Energy under W-7405-ENG-48, DE-FC02-04ER54698, DE-AC05-00OR22725, DE-AC04-94AL85000, DE-FG02-04ER54758 and DE-FG03-01ER54615.

References

[1] M.A. Mahdavi, R. Maingi, R.J. Groebner, et al., Phys. Plasmas 10 (2003) 3984.
[2] M.A. Mahdavi, J.C. DeBoo, C.L. Hsieh, et al., Phys. Rev. Lett. 47 (1981) 1602.
[3] B. LaBombard, R.L. Boivin, M. Greenwald, et al., Phys. Plasmas 8 (2001) 2107.
[4] M.E. Fenstermacher, W.H. Meyer, R.D. Wood, et al., Rev. Sci. Instrum. 70 (1997) 974.
[5] M. Groth, M.E. Fenstermacher, C.J. Lasnier, et al., Rev. Sci. Instrum. 74 (2003) 2064.
[6] R.J. Colchin, N.H. Brooks, D.L. Hillis, et al., Rev. Sci. Instrum. 74 (2003) 2068.
[7] J.G. Watkins, R.A. Moyer, J.W. Cuthbertson, et al., J. Nucl. Mater. 241–243 (1997) 645.
[8] T.N. Carlstrom, G.L. Campbell, J.C. DeBoo, et al., Rev. Sci. Instrum. 63 (1992) 4901.
[9] S.L. Allen, D.N. Hill, T.N. Carlstrom, et al., J. Nucl. Mater. 241–243 (1997) 595.
[10] T.D. Rognlien, J. Milovich, M.E. Rensick, et al., J. Nucl. Mater. 196–198 (1992) 347.
[11] D.B. Heifetz, D. Post, M. Petravic, et al., J. Comp. Phys. 46 (1982) 309.
[12] P.C. Stangeby, J.D. Elder, J.A. Boedo, et al., J. Nucl. Mater. 313–316 (2003) 883.
[13] T.D. Rognlien, G.D. Porter, D.D. Ryutov, J. Nucl. Mater. 266–269 (1999) 654.
[14] J.W. Davis, A.A. Haasz, J. Nucl. Mater. 241–243 (1997) 37.
[15] J. Neuhauser, W. Schneider, R. Wunderlich, et al., Nucl. Fus. 24 (1984) 39.
[16] L.W. Owen, R.J. Colchin, R. Maingi, et al., J. Nucl. Mater. 290–293 (2001) 464.
[17] R.J. Colchin, L.W. Owen, J. Nucl. Mater. 313–316 (2003) 806.
[18] T.W. Petrie, J.G. Watkins, L.R. Baylor, et al., J. Nucl. Mater. 313–316 (2003) 834.
[19] N.S. Wolf, T.W. Petrie, G.D. Porter, et al., J. Nucl. Mater. 313–316 (2003) 564.
[20] M.V. Umansky, S.I. Krasheninnikov, B. LaBombard, et al., Phys. Plasmas 6 (1999) 2761.
[21] A.Y. Pigarov, S.I. Krasheninnikov, T.D. Rognlien, et al., Phys. Plasmas 9 (2002) 1287.